Different Glucose Uptake and Glycolytic Mechanisms Between Hepatocellular Carcinoma and Intrahepatic Mass-Forming Cholangiocarcinoma with Increased ^{18}F-FDG Uptake

Jong Doo Lee, MD, PhD[1]; Woo Ick Yang, MD, PhD[2]; Young Nyun Park, MD, PhD[2]; Kyung Sik Kim, MD, PhD[3]; Jin Sub Choi, MD, PhD[3]; Mijin Yun, MD[1]; Dooheun Ko, MD[1]; Tae-Sung Kim, MD[1]; Arthur E.H. Cho, MD[1]; Hye Mi Kim, MD, PhD[1]; Kwang-Hyub Han, MD, PhD[4]; Seung-Soon Im, MS[5]; Yong-Ho Ahn, MD, PhD[5]; Chang Woon Choi, MD, PhD[6]; and Jeon Han Park, MD, PhD[7]

[1]Division of Nuclear Medicine, Department of Diagnostic Radiology, Yonsei University College of Medicine, Seoul, Korea; [2]Department of Pathology, Yonsei University College of Medicine, Seoul, Korea; [3]Department of Surgery, Yonsei University College of Medicine, Seoul, Korea; [4]Department of Internal Medicine, Yonsei University College of Medicine, Seoul, Korea; [5]Department of Biochemistry and Molecular Biology, Yonsei University College of Medicine, Seoul, Korea; [6]Department of Nuclear Medicine, Korea Cancer Center Hospital, Seoul, Korea; and [7]Department of Microbiology, Yonsei University College of Medicine, Seoul, Korea

^{18}F-FDG uptake in malignant tumors largely depends on the presence of facilitated glucose transporters, especially type 1 (Glut 1) and a rate-limiting glycolytic enzyme, hexokinase (HK) type II. Low expression of Glut 1 was reported in hepatocellular carcinoma (HCC), whereas high expression was found in cholangiocarcinoma. Immunohistochemistry and proteome analysis were performed to obtain a detailed evaluation of the mechanisms involved in glucose uptake and use in these tumors. **Methods:** Tumor tissues obtained from both HCC ($n = 7$) and mass-forming cholangiocarcinoma patients ($n = 7$) who showed increased ^{18}F-FDG uptake on PET were used. Immunohistochemistry for Glut 1 and HK I–III was performed in all tumor tissues. To identify proteins that regulate carbohydrate metabolism, a proteome analysis with matrix-assisted laser desorption ionization–time of flight and enzymatic digestion in-gel were performed using 8 available tumor samples and 3 normal liver tissues. Of the 8 tumor samples, 4 were HCCs; one was an intermediate phenotype HCC, and 3 were cholangiocarcinomas. The spot intensity of the proteins was calculated using proteome data; the tissues then were divided into 2 groups on the basis of the protein expression pattern, because the protein expression pattern of the intermediate-phenotype HCC was close to that of the cholangiocarcinomas. Group A included the HCCs and group B included the intermediate-phenotype HCC as well as the cholangiocarcinomas. **Results:** Immunoreactivity for Glut 1 was positive in all cholangiocarcinomas, but was negative in all HCCs except the one intermediate phenotype. However, HK II was positive in HCCs but was negative in 6 of the 7 cholangiocarcinomas. A total of 331 protein spots with a P value of <0.05 were identified by proteome analysis. Thirteen of these proteins that regulate carbohydrate metabolism were selected. The pentose phosphate pathway was increased in both groups, but more significantly in group B. Gluconeogenesis enzymes were decreased in both groups, but the tricarboxylic acid cycle–regulating enzyme expression was variable. **Conclusion:** HCCs have different glucose-regulating mechanisms from those of cholangiocarcinomas, even though both tumors showed increased ^{18}F-FDG uptake on PET scans. Further studies are required with regard to energy metabolism and ^{18}F-FDG uptake patterns in association with various oncogenic alterations regulating multiple steps of the glycolytic pathways.

Key Words: ^{18}F-FDG; glucose metabolism; hepatocellular carcinoma; cholangiocarcinoma

J Nucl Med 2005; 46:1753–1759

In past years, ^{18}F-FDG PET has been widely used clinically in the field of oncology because of its high sensitivity and specificity, and it also has significant potential for assessing therapy response (1). Because cancer cell growth is heavily dependent on glucose metabolism as a major energy substrate, the ^{18}F-FDG uptake pattern on PET scans that reflects glycolytic activity could be an indicator of the prognosis and aggressiveness of the tumors. In addition, the association of neoplastic growth with increased aerobic glycolysis has been known as the Warburg effect for more

than 7 decades (*2*). However, ¹⁸F-FDG uptake patterns in primary hepatic tumors are variable. Increased uptake can be seen in only half of hepatocellular carcinoma (HCC) patients (*3*); mass-forming intrahepatic cholangiocarcinomas show intense ¹⁸F-FDG uptake, whereas hilar cholangiocarcinomas show only mild uptake (*4*).

In our previous study, the ¹⁸F-FDG uptake was closely correlated with the pathologic grading in HCC. HCCs with increased ¹⁸F-FDG uptake showed molecular features of more aggressive biologic properties than those with a low ¹⁸F-FDG uptake (*5*). However, the glucose uptake pattern and its clinical implications have not been evaluated in cholangiocarcinomas.

¹⁸F-FDG uptake in malignant tumors depends largely on the presence of facilitated glucose transporters, including type 1 (Glut 1) and a rate-limiting glycolytic enzyme, hexokinase (HK) type II (*6*). In previous reports, it was demonstrated that Glut 1 is highly expressed in cholangiocarcinomas but rarely expressed in HCCs (*7,8*). In contrast, HK II expression is increased in HCCs (*9*) but unknown in cholangiocarcinomas. These findings suggest that glucose uptake and glycolytic mechanisms could differ between HCCs and cholangiocarcinomas, even though both tumors use glucose as a major energy source. To explore the differences of mechanisms involving glucose uptake and glycolysis in these tumors, immunohistochemistries for Glut 1 and HK I–III were performed as well as proteome analysis of the enzymes regulating the glucose metabolism using the tumor tissues obtained from HCC and mass-forming cholangiocarcinoma patients showing increased ¹⁸F-FDG uptake on PET scans.

MATERIALS AND METHODS

Tissue Specimens

Tumor tissue specimens from 14 patients (7 HCCs and 7 cholangiocarcinomas) who had undergone partial hepatectomy were obtained and stored in a deep freezer ($-70°C$) for proteomic analysis or embedded in paraffin for hematoxylin–eosin staining and immunohistochemistry. The age of the patients ranged from 40 to 73 y. All tumor tissues demonstrated increased ¹⁸F-FDG uptake on a PET scan (standardized uptake values [SUVs] of ¹⁸F-FDG ranged from 3.2 to 17.4). Approval was obtained from the Ethical Committee in our institute for this study.

PET Procedure

Before surgery, all patients were examined with a whole-body PET camera (Advance; GE Healthcare). Before scanning, patients fasted for at least 6 h, and their plasma glucose concentrations were measured. The blood glucose level was <140 mg/dL. Approximately 370 MBq ¹⁸F-FDG were injected intravenously, and the emission scan (5 min/bed) was started from the neck to the knee in 2-dimensional (2D) mode 50–60 min after the injection. Patients then underwent a transmission scan (3 min/bed) with rotating ⁶⁸Ge sources. The images were reconstructed with the attenuation-corrected ordered-subset expectation maximization algorithm (number of subsets, 16; number of iterations, 2). The PET scans were compared with the corresponding CT or MR images for an accurate localization of the tumors. The coronal, sagittal, and axial images of the patients were qualitatively evaluated to determine whether the ¹⁸F-FDG uptake in the tumor was higher than that in the surrounding noncancerous hepatic tissue. For a semiquantitative evaluation, a small region of interest (8 pixels) was placed over the area of maximum ¹⁸F-FDG uptake in the tumors and the maximum SUV (SUV_{max}) normalized to body weight was calculated.

Immunohistochemistry

Hematoxylin–eosin staining of 5-μm-thick paraffin sections was performed and sections were then deparaffinized and rehydrated for immunohistochemistry. After wax removal and dehydration, sections were pretreated in a 0.01 mol/L citrate buffer (pH 6.0) using a microwave oven (820 W, 15 min) for antigen retrieval. They were then incubated with primary antibodies at 4°C overnight. These primary antibodies were polyclonal human anti-Glut 1, rat antihexokinase type II, monoclonal anti-HK type I and type III (Chemicon International Inc.), and monoclonal anticytokeratin (CK)-19 (Dako). The antibodies were diluted to 1:1,000, 1:5,000, 1:100, 1:200, and 1:50, respectively. Endogenous peroxidase activity was blocked by incubation in H_2O_2 for 10 min. After washing, signals were detected using an EnVision Kit (Dako) and diaminobenzidine. The presence of membrane-bound Glut 1 and intracytoplasmic HK I–III was examined for all tumor tissues, and CK-19 was evaluated in HCCs for further classification of HCCs into a primary HCC and an intermediate (hepatocyte-cholangiocyte) phenotype (*10*). Sections incubated with preimmune serum served as negative controls. Red blood cells present in the tissues and rat skeletal muscle served as positive controls for Glut 1 and hexokinases, respectively,

Proteome Analysis

An adequate amount of protein was obtained from 8 tumor specimens (5 HCCs and 3 cholangiocarcinomas) and 3 adjacent normal tissues. Proteome analysis was undertaken using these samples.

Reagents. Urea, thiourea, 3-([3-cholamidopropy]dimethyammonio)-1-propanesulfonate (CHAPS), dithiothreitol (DTT), benzamidine, Bradford solution, acrylamide, iodoacetamide, bisacrylamide, sodium dodecylsulfate (SDS), acetonitrile, trifluoroacetic acid, and α-cyano-4-hydroxycinnamic acid were purchased from Sigma-Aldrich. Pharmalyte (pH 3.5–10) was from Amersham Biosciences and immobilized pH gradient (IPG) DryStrips (pH 4–10; nonlinear, 24 cm) were from Genomine Inc. Modified porcine trypsin (sequencing grade) was from Promega.

Protein Sample Preparation. Tissue samples were washed twice in ice-cold phosphate-buffered saline, blotted to dry, and directly homogenated using a motor-driven homogenizer (Fisher Scientific) with a sample buffer containing 7 mol/L urea, 2 mol/L thiourea (containing 4% [w/v] CHAPS, 1% [w/v] DTT, and 2% [v/v] pharmalyte), and 1 mmol/L benzamidine. Proteins were extracted for 1 h at room temperature. After being centrifuged at 15,000*g* for 1 h at 15°C, the insoluble material was discarded and the soluble fraction was used for a 2D gel electrophoresis. In addition, a membrane fraction was obtained after centrifuging the sample at 1,400*g*. Protein loading was normalized using a Bradford Assay (*11*).

2D Polyacrylamide Gel Electrophoresis (PAGE). IPG dry strips were equilibrated for 12–16 h with sample buffer containing 7 mol/L urea and 2 mol/L thiourea (containing 2% CHAPS, 1% DTT, and 1% pharmalyte) and loaded with 200 μg of sample. Isoelectric focusing (IEF) was performed at 20°C using a Mul-

tiphor II electrophoresis unit and an EPS 3500 XL power supply (Amersham Biosciences) following the manufacturer's instructions. For IEF, the voltage was increased linearly from 150 to 3,500 V for 3 h to allow for sample entry. This was followed by a constant 3,500 V, with focusing complete after 96 kVh. Before the second dimension, strips were incubated for 10 min in an equilibration buffer (50 mmol/L Tris-Cl, pH 6.8, containing 6 mol/L urea, 2% SDS, and 30% glycerol), first with 1% DTT and then with 2.5% iodoacetamide. The equilibrated strips were inserted into SDS–PAGE gels (20–24 cm, 10%–16%). SDS–PAGE was performed using the Hoefer DALT 2D system (Amersham Biosciences) following the manufacturer's instructions. Two-dimensional gels were run at 20°C for 1.7 kVh and then silver stained as described by Oakley et al. (12).

Image Analysis. A quantitative analysis of digitized images was performed using PDQuest software, version 7.0 (BioRad). The quantity of each spot was normalized by total valid spot intensity.

Enzymatic Digestion of Protein In-Gel. Protein spots were digested in-gel using modified porcine trypsin in a manner similar to that previously described by Shevchenko et al. (13). The gel pieces were washed with 50% acetonitrile to remove any remaining SDS, salt, and stain, Next, the pieces were dried to remove any solvent, then rehydrated with trypsin (8–10 ng/μL) and incubated for 8–10 h at 37°C. The proteolytic reaction was terminated by the addition of 5 μL 0.5% trifluoroacetic acid. Peptides were recovered by combining the aqueous phases obtained from extracting pieces of gel with 50% aqueous acetonitrile. After concentration, the peptide mixture was desalted using C_{18}ZipTips (Millipore) and eluted in 1–5 μL of acetonitrile. An aliquot of this solution was mixed with an equal volume of a saturated solution of α-cyano-4-hydroxycinnamic acid in 50% aqueous acetonitrile, and 1 μL of the mixture was spotted onto a target plate.

Matrix-Assisted Laser Desorption Ionization–Time-of-Flight (MALDI–TOF) Analysis and Database Search. A protein analysis was performed using MALDI–TOF (Amersham Biosciences). Peptides were evaporated with an N2 laser at 337 nm using a delayed extraction approach. They were accelerated with a 20-kV injection pulse to analyze the time of flight. Each spectrum was the cumulative average of 300 laser shots. The search program Pro-Found, developed by Rockefeller University (http://129.85.19.192/profound_bin/WebProFound.exe), was used for protein identification using peptide mass fingerprinting. Spectra were calibrated with the trypsin autodigestion ion peaks m/z (842.510, 2211.1046) as internal standards.

Data Analysis. Tumor specimens were divided into 2 groups on the basis of their protein expression patterns. HCCs were part of group A, whereas group B included the intermediate-phenotype HCC and the cholangiocarcinomas, because the protein expression pattern of the intermediate-phenotype HCC was close to that of the cholangiocarcinoma group (Figs. 1A and 1B). Comparisons between the 2 characteristics (normal vs. group A, normal vs. group B, and group A vs. group B) were assessed using a Student t test, and relationships were considered statistically significant when $P < 0.05$. Relative spot intensity (tumor/normal) was calculated in each group for comparison.

Reverse Transcription–Polymerase Chain Reaction (RT–PCR)

Total RNA was successfully isolated from 2 HCCs including the intermediate phenotype, 2 cholangiocarcinomas, and 3 adjacent normal liver tissues using a Trizol reagent (Introgen) as directed by the manufacturer's protocol. Messenger RNA (mRNA) expression of the first reaction enzyme in the pentose phosphate pathway (PPP)—that is, glucose-6-phosphate dehydrogenase (G6PDH)—was evaluated. First-strand complementary DNA was synthesized from 3 μL of the total RNA using random hexamer and Superscript II reverse transcriptase (Life Technologies). One microliter of the reverse transcription reaction mixture was amplified with primers specific for G6PDH, and glyceraldehyde 3-phosphate dehydrogenase (GAPDH) as an internal control in the total volume of 50 μL. Linearity of the PCR was tested by amplification cycles between 25 and 30. Primers used in PCR were as follows:
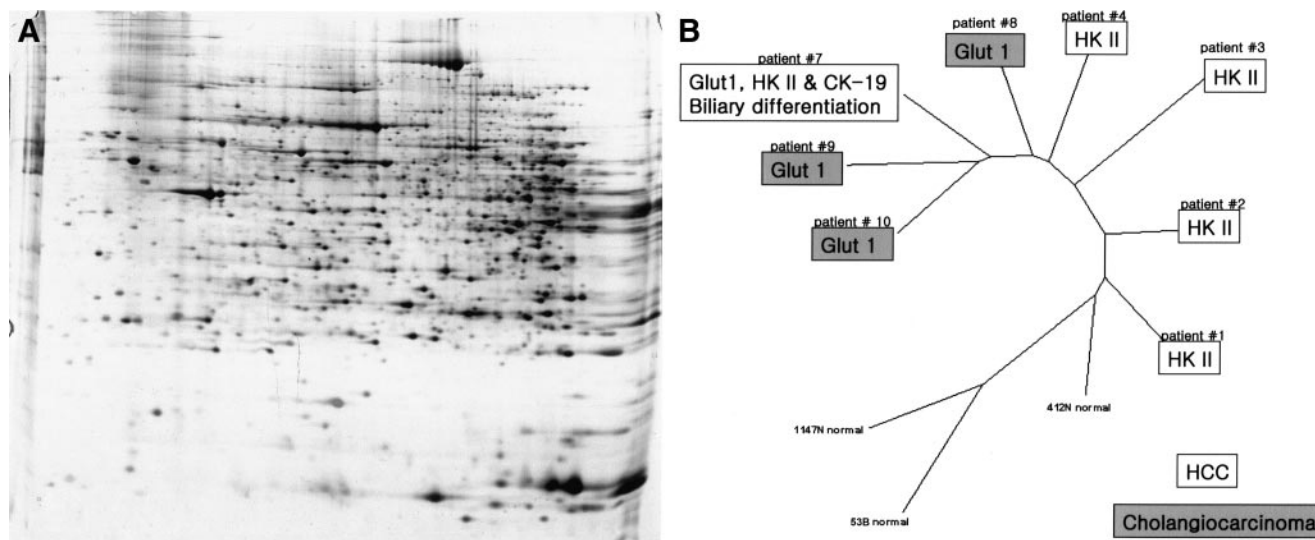

FIGURE 1. (A) Two-dimensional gel electrophoresis map of human liver tumor tissue demonstrates numerous protein spots. (B) Proteome analysis enables grouping of tumors (normal, HCC, and cholangiocarcinoma groups) as seen on distance tree mapping of protein expression profiles. However, protein expression pattern of intermediate phenotype of HCC group (patient 7) is close to cholangiocarcinoma group.

Patient no.	Age (y)	Sex	Pathology	SUV	Glut 1	HK I	HK II	HK III
1	40	M	HCC, G II–III	3.3	−	−	+	−
2	54	M	HCC, G III	3.9	−	−	+	−
3	54	M	HCC, G II–III	5.6	−	Weak	+	Weak
4	50	M	HCC, G III, HB cirrhosis	3.2	−	−	+	−
5	58	F	HCC, G II–III, HB cirrhosis	7.3	−	−	+	−
6	63	F	HCC, G III, HB cirrhosis	3.8	−	−	+	−
7	53	F	Intermediate HCC, HB cirrhosis	10.0	+	−	+	−
8	41	F	Cholangiocarcinoma, MD	13.4	+	−	−	−
9	48	F	Cholangiocarcinoma, MD	9.1	+	−	−	−
10	52	M	Cholangiocarcinoma, MD	13.5	+	−	−	Weak
11	47	F	Cholangiocarcinoma, PD	8.7	+	−	−	−
12	73	M	Cholangiocarcinoma, MD	6.2	+	−	Weak	−
13	75	M	Cholangiocarcinoma, PD	12.8	+	−	−	−
14	54	F	Cholangiocarcinoma, PD	17.4	+	−	−	Weak

G = grade; HB = hepatitis B; MD = moderately differentiated; PD = poorly differentiated.

- G6PDH-sense, 5′-ACCTGGCCAAGAAGAAGATC-3′,
- G6PDH-antisense, 5′-TAGGAGGCTGCATCATCGTA-3′,
- GAPDH-sense, 5′-ACCAC AGTCC ATGCC ATCAC-3′,
- GAPDH-antisense, 5′-TCCAC CACCC TGTTG CTGTA-3′.

RESULTS

Immunohistochemistry

Immunoreactivity for Glut 1 was positive in all cholangiocarcinomas but was negative in all HCCs except one (Table 1). In contrast, HK II was positive in HCCs but was negative in 6 of 7 cholangiocarcinomas (Figs. 2 and 3). CK-19 was positive only in the HCC, which had positive reactions for both Glut 1 and HK II. This is consistent with the intermediate phenotype of HCC (Fig. 4).

HK I was weakly positive in only one HCC, and HK-III was weakly positive in one HCC and 2 cholangiocarcinomas.

Protein Expression Profiles

A total of 331 protein spots that had a *P* value of <0.05 were selected for identification. Thirteen proteins involved in the metabolism of carbohydrates were chosen from this total for comparison and were classified as shown in Table 2.

PPP. The expression of 6-phosphogluconolactonase, the second step enzyme in the PPP, was markedly increased in group B (Fig. 5). Although G6PD, the first step-regulating enzyme, was not identified on proteome analysis, mRNA expression on the RT–PCR significantly increased as the 6-phosphogluconolactonase protein expression pattern (Fig. 6).

Tricarboxylic Acid (TCA) Cycle. Six enzymes of 8 successive reaction steps in the TCA cycle were differentially expressed. Isocitrate dehydrogenase (3rd-step reaction enzyme) and β-succinyl CoA synthetase (5th-step reaction enzyme) were increased, whereas α-ketoglutarate dehydrogenase (4th-step reaction enzyme), succinate dehydrogenase (6th-step reaction enzyme), and fumarase (7th-step reaction enzyme) were decreased in both groups, more significantly in group B. Pyruvate carboxylase involving in
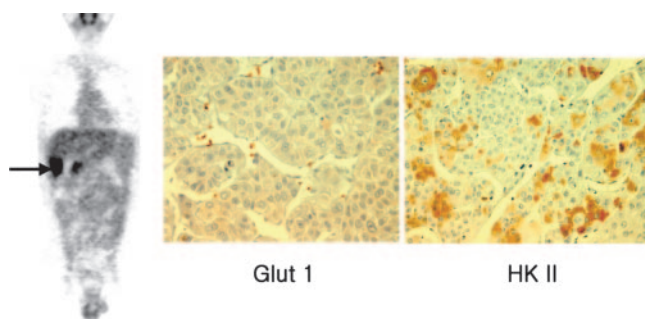
FIGURE 2. Nodular HCC (Edmondson grade II–III) in right lobe of liver, inferior segment, shows increased ^{18}F-FDG uptake on PET scan (patient 3). Immunohistochemical staining shows a negative reaction for Glut 1 but a positive reaction for HK II (×400).
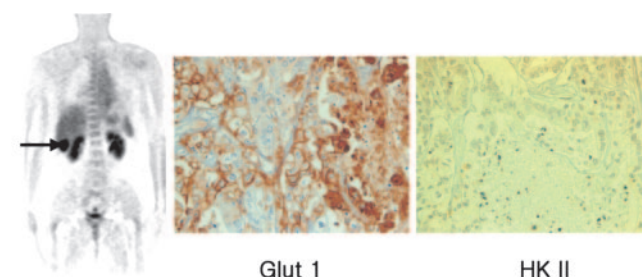
FIGURE 3. Mass-forming cholangiocarcinoma in right lobe of liver, inferior segment, shows intense ^{18}F-FDG uptake (patient 10). Pathologically, tumor shows a strong positive reaction for Glut 1 along cell membrane but a negative reaction for HK II (×400).
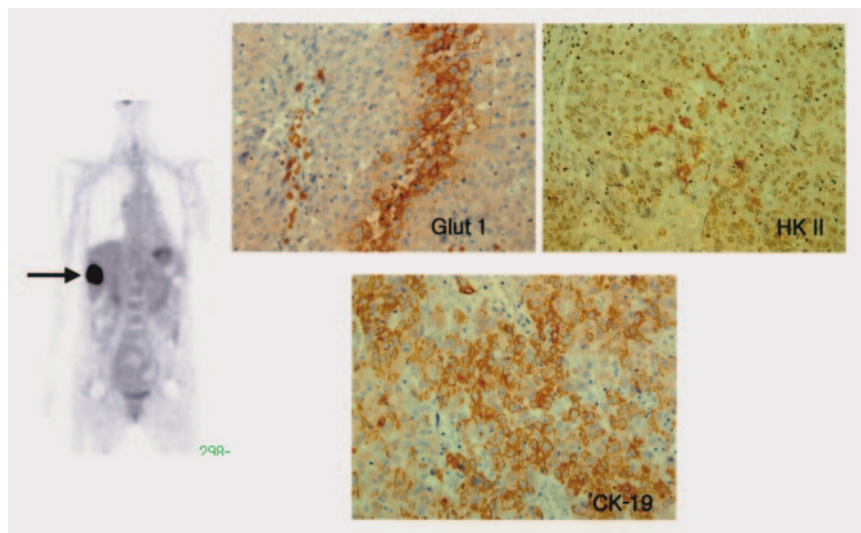
FIGURE 4. Mass with intense ^{18}F-FDG uptake as seen in Figures 2 and 3 shows a positive reaction for both Glut 1 and HK II and, additionally, the biliary marker CK-19 (patient 7) ($\times$400). Morphologically, lesion is classified as an HCC; however, biologically, it has both HCC and cholangiocarcinoma phenotypes.

anaplerotic reaction increased in group A but decreased in group B.

Gluconeogenesis. Glyoxalate reductase/hydroxypyruvate reductase was decreased in group B, and phosphoenolpyruvate carboxykinase (PEPCK) was decreased in both groups, but was more pronounced in group A.

Others. Pyruvate kinase, mannosephosphate isomerase, citrate lyase, and ketohexokinase decreased in both groups. Glutathione peroxidase (GPO), which is essential in the normal detoxification of H_2O_2, was increased in both groups. This increase was higher in group B (Fig. 5).

Glut 1 and HK proteins could not be identified on proteome analysis, possibly due to technical difficulties en-

countered during the extraction of membranous proteins (*14*).

DISCUSSION

Hepatocyte origin HCCs and bile duct origin cholangiocarcinomas are the major primary hepatic carcinomas. Although both high-grade HCCs and intrahepatic mass-forming cholangiocarcinomas showed high rates of glycolysis—that is, increased ^{18}F-FDG uptake on PET scans—our results demonstrated that the mechanisms involved in glucose uptake and glycolytic metabolism appear to be different from each other.

TABLE 2
Proteins Involved in Carbohydrate Metabolism

Protein	Accession no.	Spot ratio (tumor/normal)		Function
		Group A	Group B	
PPP				
6-Phosphogluconolactonase	NP_036220	1.2	2.5	6-Phosphogluconolactone→6-phosphogluconate
TCA cycle				
Pyruvate carboxylase	P 11498	2.0	0.3	Anaplerotic reaction, pyruvate→oxaloacetate
Isocitrate dehydrogenase	NP_005521	2.6	3.5	TCA cycle (3rd step), isocitrate→α-ketoglutarate
α-Ketoglutarate dehydrogenase	AAH 26320	0.7	0.1	TCA cycle (4th step), α-ketoglutarate→succinyl CoA
β-Succinyl CoA synthetase	AAP 97189	1.8	2.5	TCA cycle (5th step), succinyl CoA→succinate
Succinate dehydrogenase	P31040	0.4	0.2	TCA cycle (6th step), succinate→fumarate
Fumarase	NP_000134	0.7	0.5	TCA cycle (7th step), fumarate→malate
Gluconeogenesis				
Phosphoenolpyruvate carboxykinase	A45746	0.1	0.4	Phosphoenolpyruvate→oxaloacetate
Glyoxylate reductase	NP_036335	1.0	0.2	Serine→glucose
Others				
Mannosephosphate isomerase	NP_002426	1.3	2.4	Mannose-6-phosphate→fructose-6-phosphate
Pyruvate kinase	NP_870986	0.4	0.2	Phosphoenolpyruvate→pyruvate
Citrate lyase	AAL84703	0.7	0.3	Citrate→acetyl CoA
Ketohexokinase	CAA55346	0.7	0.1	Fructose→fructose-1-phosphate

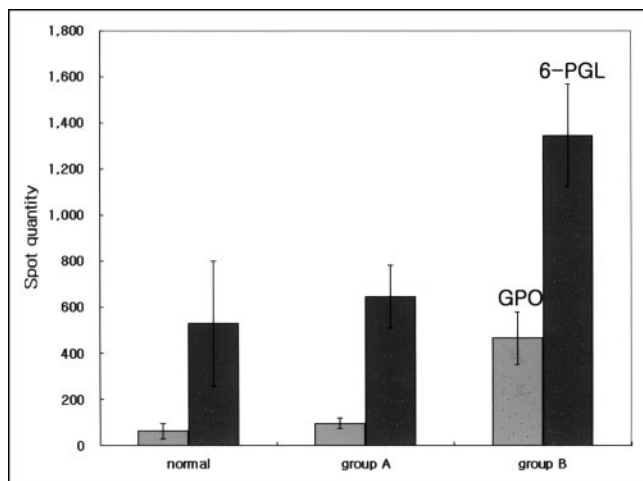PPP = pentose phosphate pathway; TCA = tricarboxylic acid; CoA = coenzyme A.

FIGURE 5. Protein expression level of glutathione peroxidase (GPO) and especially 6-phosphogluconolactonase (6-PGL) is increased in both HCC and cholangiocarcinomas, more in cholangiocarcinoma group. (Group A includes HCCs; group B includes intermediate phenotype of HCC and cholangiocarcinomas.)

Although most malignant cells highly express glucose transporters, especially Glut 1 (6,15), it is not increased in HCCs (7), as was seen in our study. The exact mechanisms have not been fully evaluated, but previous reports have revealed that the growth of HCCs is glutamine dependent (16,17), and fatty acids are the major energy source in HCC cells (18). These findings might be possible explanations for the low incidence of Glut 1 expression and lower ^{18}F-FDG uptake in HCCs compared with cholangiocarcinomas.

In addition to Glut 1, HKs—the first rate-limiting enzymes of the glycolytic pathway—also play a pivotal role in ^{18}F-FDG uptake and glycolytic pathways in malignant cells. Among the 4 hexokinase isozymes in mammalian tissues (HK I–IV), HK II is markedly increased in rapidly growing, highly malignant tumors, including HCCs (19,20). Additionally, an isozyme shift from type IV (glucokinase) to HK II has been observed in HCCs (21,22). However, most of the cholangiocarcinoma tissues did not demonstrate increased expression of HK II despite high ^{18}F-FDG uptake. The mechanisms of low expression of HK II in cholangiocarcinoma were not investigated, but previous data demonstrated that glucose-6-phosphate production depends more on the phosphorylating enzyme activity of HK II than on the protein expression level (23) and hexokinase is inhibited by the increased concentration of intracellular glucose-6-phosphate, which suggests that ^{18}F-FDG uptake does not always parallel the HK protein expression level. However, in conditions in which carbohydrates are limiting, as is seen in HCCs (24), it is important to have an increased amount of HK II protein, especially the mitochondrial bond form for efficient glucose use in cancer cells. In fact, mitochondrial-bound hexokinase accounts for as much as 70% of the total cellular hexokinase in hepatoma cells, whereas the amount found on the mitochondria in normal liver cells is negligible

(25). HK II bound to porins on the outer mitochondrial membrane prevents apoptosis via Bax-induced inhibition of cytochrome c release (26), Bax conformation change, and BID cleavage in association with activated serine/threonine kinase Akt/PKB (Akt) (27,28).

Glucose-6-phosphate produced by HK II can be used for lactate production, glycogen synthesis, the PPP for lipid or nucleotide synthesis, and also reduced nicotinamide adenine dinucleotide phosphate (NADPH) generation to maintain the redox state of the tumor cells under oxidative stress. However, use of glucose-6-phosphate for oxidative phosphorylation via the TCA cycle is relatively lower than for glycolysis or the PPPs as described previously (29–31).

In our study, both tumors showed an increase in the expression of the second-step enzyme, 6-phosphogluconolactonase, in terms of the PPP. The increase was greater in group B. Although the first-step enzyme, G6PDH, was not identified by proteome analysis—probably due to failure in protein solubilization during the IEF step (14)—mRNA expression was markedly increased in group B on RT–PCR. These findings may support the fact that the PPP plays an important role in cancer cell survival in cholangiocarcinomas or intermediate-phenotype HCCs. NADPH generated by enhanced pentose phosphate shunt produces the reduced form glutathione (GSH) from the oxidized form (GSSH); therefore, it further activates 6-phosphogluconolactonase activity (32). Moreover, glutathione peroxidase, which renders the cells resistant to H_2O_2, was overexpressed in our study, particularly in group B. This appears to be an additional cellular protective mechanism against oxidative stress.

The enzyme expression pattern involved in the TCA cycle was variable. Fluctuation in the concentration of key metabolites such as glutamine and glutamate, which reflect the cellular balance between adenosine triphosphate production and consumption, could have caused these enzyme expression variations. The clinical implications of metabolic regulations in the TCA cycle were not fully investigated in these tumors. Further studies are required.
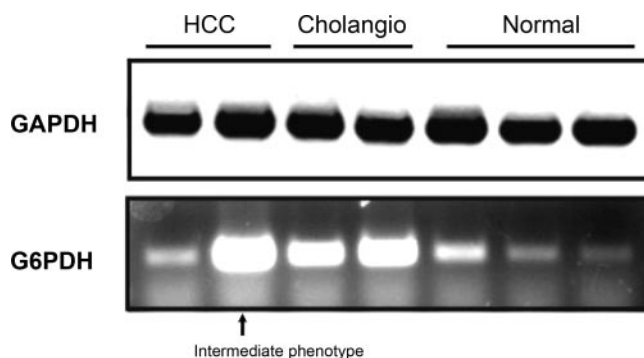

FIGURE 6. mRNA expression of glucose-6-phosphate dehydrogenase (G6PDH) is markedly increased in intermediate-phenotype HCC and cholangiocarcinomas (Cholangio) compared with normal and HCC.

Gluconeogenic enzymes such PEPCK were diminished in both groups, which is concordant with a previous report (*33*), and activation of Akt is known to be sufficient to repress the glucocorticoid and cyclic adenosine monophosphate–stimulated increase in PEPCK gene transcription (*34*).

An intriguing finding in our study was that the protein expression pattern in the intermediate phenotype of HCCs was quite close to that of cholangiocarcinomas. Detailed molecular and biologic analysis in this particular type of cancer is required for a better understanding of the tumor characteristics and behaviors.

CONCLUSION

HCCs have different glucose-regulating mechanisms and enzyme expression pattern than those of cholangiocarcinomas, even though both tumors show similarity in the enhanced glucose uptake pattern on PET scans. Further studies are required with regard to the energy metabolism and ^{18}F-FDG uptake patterns in association with various oncogenic alterations, because the tumor-suppressor genes p53, H-ras, HIF-α, c-myc, and Akt regulate glucose use in multiple steps of the glycolytic pathways (*35*).

REFERENCES

1. Kelloff GJ, Hoffman JM, Johnson B, et al. Progress and promise of FDG-PET imaging for cancer patient management and oncologic drug development. *Clin Cancer Res.* 2005;11:2785–2808.
2. Warburg O. On the origin of cancer cells. *Science.* 1956;123:309–314.
3. Ho CL, Yu CH, Yeung DWC. ^{11}C-Acetate PET imaging in hepatocellular harcinoma and other liver masses. *J Nucl Med.* 2003;44:213–222.
4. Kim YJ, Yun M, Lee WJ, Kim KS, Lee JD. Usefulness of ^{18}F-FDG PET in intrahepatic cholangiocarcinoma. *Eur J Nucl Med Mol Imaging.* 2003;30:1467–1472.
5. Lee JD, Yun M, Lee JM, et al. Analysis of gene expression profiles of hepatocellular carcinomas with regard to F-18-FDG uptake pattern on positron emission tomography. *Eur J Nucl Med Mol Imaging.* 2004;31:1621–1630.
6. Higashi T, Saga T, Nakamoto Y, et al. Relationship between retention index in dual-phase ^{18}F-FDG PET, and hexokinase-II and glucose transporter-1 expression in pancreatic cancer. *J Nucl Med.* 2002;43:173–180.
7. Roh MS, Jeong JS, Kim YH, Kim MC, Hong SH. Diagnostic utility of GLUT 1 in the differential diagnosis of liver carcinomas. *Hepatogastroenterology.* 2004;51:1315–1318.
8. Zimmerman RL, Fogt F, Burke M, Murakata LA. Assessment of Glut-1 expression in cholangiocarcinoma, benign biliary lesions and hepatocellular carcinoma. *Oncol Rep.* 2002;9:689–692.
9. Mathupala SP, Rempel A, Pedersen PL. Glucose catabolism in cancer cells: isolation, sequence, and activity of the promotor type II hexokinase. *J Biol Chem.* 1995;270:16918–16925.
10. Kim H, Park C, Han KH, et al. Primary liver carcinoma of intermediate (hepatocyte-cholangiocyte) phenotype. *J Hepatol.* 2004;40:298–304.
11. Bradford NM. A rapid and sensitive method for the quantitation of microgram quantities of protein utilizing the principle of protein-dye binding. *Anal Biochem.* 1976;72:248–254.
12. Oakley BR, Kirsch DR, Morris NR. A simplified ultrasensitive silver stain for detecting proteins in polyacrylamide gels. *Anal Biochem.* 1980;105:361–363.
13. Shevchenko A, Wilm M. Vorm O, Mann M. Mass spectrometric sequencing of proteins in silver-stained polyacrylamide gels. *Anal Chem.* 1996;68:850–858.
14. Santoni V, Molloy M, Rabilloud T. Membrane proteins and proteomics: Un amour impossible? *Electrophoresis.* 2000;21:1054–1070.
15. Larson SM. Positron emission tomography-based molecular imaging in human cancer: exploring the link between hypoxia and accelerating glucose metabolism. *Clin Cancer Res.* 2004;10:2203–2204.
16. Wong MS, Raab RM, Rigoutsos I, Stephanopoulos GN, Kelleher JK. Metabolic and transcriptional patterns accompanying glutamine depletion and repletion in mouse hepatoma cells: a model for physiological regulatory networks. *Physiol Genomics.* 2004;16:247–255.
17. Bode BP, Fuchs BC, Hurley BP, et al. Molecular and functional analysis of glutamine uptake in human hepatoma and liver-derived cells. *Am J Physiol Gastrointest Liver Physiol.* 2002;283:G1062–G1073.
18. Hansson PK, Asztely AK, Clapham JC, Schreyer SA. Glucose and fatty acid metabolism in McA-RH7777 hepatoma cells vs. rat primary hepatocytes: responsiveness to nutrient availability. *Biochim Biophys Acta.* 2004;1684:54–62.
19. Wilson JE. Isozymes of mammalian hexokinases: structure, subcellular localization and metabolic function. *J Exp Biol.* 2003;206:2049–2057.
20. Goel A, Mathupala SP, Pedersen PL. Glucose metabolism in cancer: evidence that methylation events play a role in activating type II hexokinase gene expression. *J Biol Chem.* 2003;278:15333–15340.
21. Klimek F, Bannasch P. Isozyme shift from glucokinase to hexokinase is not an early but a late event in hepatocarcinogenesis. *Carcinogenesis.* 1993;14:1857–1861.
22. Rencurel F, Munose-Alonso MJ, Girard J, Leturque A. An unusual high K_m hexokinase is expressed in the mhAT3F hepatoma cell line. *J Biol Chem.* 1998;273:26187–26193.
23. Aloj L, Caraco C, Jagoda E, Eckelman WC, Neuman RD. Glut-1 and hexokinase expression: relationship with 2-fluoro-2-deoxy-D-glucose uptake in A431 and T47D cells in culture. *Cancer Res.* 1999;59:4709–4714.
24. Rempel A, Mathupala SP, Pedersen PL. Glucose catabolism in cancer cells: regulation of the type II hexokinase promoter by glucose and cyclic AMP. *FEBS Lett.* 1996;385:233–237.
25. Parry DM, Pedersen PL. Intracellular localization and properties of particulate hexokinase in the Novikoff ascites tumor: evidence for an outer mitochondrial membrane location. *J Biol Chem.* 1983;258:10904–10912.
26. Pastorino JG, Shulga N, Hoek JB. Mitochondrial binding of hexokinase II inhibits Bax-induced cytochrome c release and apoptosis. *J Biol Chem.* 2003;277:7610–7618.
27. Rathmell JC, Fox CJ, Plas DR, Hammerman PS, Cinalli RM, Thompson CB. Akt-directed glucose metabolism can prevent Bax conformation change and promote growth factor-independent survival. *Mol Cell Biol.* 2003;23:7315–7328.
28. Majewski N, Nogueira V, Robery RB, Hay N. Akt inhibits apoptosis downstream of BID cleavage via a glucose-dependent mechanism involving mitochondrial hexokinases. *Mol Cell Biol.* 2004;24:730–740.
29. Elstrom RL, Bauer DE, Buzzai M, et al. Akt stimulates aerobic glycolysis in cancer cells. *Cancer Res.* 2004;64:3892–3899.
30. Hacker HJ, Sreingerg P, Toshkov I, Oesch F, Bannasch P. Persistence of cholangiocellular and hepatocellular lesions observed in rats fed a choline-deficient/DL-ethionine-supplemented diet. *Carcinogenesis.* 1992;13:271–276.
31. Frederiks WM, Bosch KS, De Jong JSSG, Van Noorden CJF. Post-translational regulation of glucose-6-phosphate dehydrogenase activity in (pre)neoplastic lesions in the rat liver. *J Histochem Cytochem.* 2003;51:105–112.
32. Fratelli M, Demol H, Puype M, et al. Identification by redox proteomics of glutathionylated proteins in oxidative-stressed human T lymphocytes. *Proc Natl Acad Sci USA.* 2002;99:3505–3510.
33. Hammond KD, Balinsky D. Activities of key gluconeogenic enzymes and glycogen synthase in rat and human livers, hepatomas, and hepatoma cell cultures. *Cancer Res.* 1978;38:1317–1322.
34. Liao J, Barthel A, Nakatani K, Roth RA. Activation of protein kinase B/Akt is sufficient to repress the glucocorticoid and cAMP induction of the phosphoenolpyruvate carboxylase gene. *J Biol Chem.* 1998;273:27320–27324.
35. Dang CV, Semenza GL. Oncogenic alteration of metabolism. *Trends Biochem Sci.* 1999;24:68–72.